

Article

Promoted Formation of Photoactive α -Formamidinium Cesium Lead Triiodide Perovskite Crystals by Germanium Addition

Ayu Enomoto, Atsushi Suzuki , Takeo Oku *  and Haruto Shimada

Department of Materials Chemistry, The University of Shiga Prefecture, 2500 Hassaka, Hikone 522-8533, Shiga, Japan

* Correspondence: oku@mat.usp.ac.jp

Abstract: Germanium (Ge) was added to formamidinium cesium lead triiodide perovskite crystals and the microstructures and photovoltaic properties were investigated. The Ge addition stabilized the α -phase of the perovskites and suppressed formation of the δ -phase. X-ray diffraction peaks of the α -phase increased by increasing the Ge contents. The highest conversion efficiency of 6.05% was obtained for the 12.5% Ge added device in an air atmosphere and the increase of efficiencies would be due to the promoted formation of photoactive α -formamidinium cesium lead triiodide perovskite crystals.

Keywords: perovskite solar cell; germanium; FAPbI₃; first principle calculation

1. Introduction

Perovskite solar cells are being investigated worldwide as the next-generation solar cells due to their simple fabrication processes and high conversion efficiencies [1–3]. Two major problems of the perovskite solar cells for the practical use are instability of the perovskite compounds and toxicity of lead (Pb), and the amount of Pb must be reduced [4–7]. Among various perovskite halides, α -phases of formamidinium cesium lead triiodide (FA_{1-y}Cs_yPbI₃) crystals have provided high efficiencies and stabilities [8,9]. However, formation of a photoinactive δ -phase of formamidinium triiodide (FAPbI₃) perovskite crystals should be suppressed and fabrication conditions of the thin films should be optimized [10–13].

Reduction of Pb is another important issue. Substitutions of Pb with other elements have been investigated not only to reduce the toxicity but also to optimize the electronic structures for improving the photovoltaic properties and stabilities. Addition of a small amount of Sn to FA_{1-y}Cs_yPbI₃ perovskite crystals suppressed the phase transition from the α -phase to δ -phase, resulting in longer carrier lifetime [14]. Germanium (Ge), a group 14 element like Pb, is also expected to suppress the photoinactive δ -phase as a substitute element for Pb [6,15]. CsPb_{1-x}Ge_xI₃ and CsPb_{1-x}Ge_xI₂Br were also investigated [16,17], which indicated that the Ge additions lowered the fabrication temperature to 90 °C and improved the stability in air for 7 h, respectively. Although several works have been reported on the substitution of Ge for these CsPbI_{3-x}Br_x compounds, it would be also interesting to investigate the substitution of Ge for formamidinium-based perovskite crystals.

The purpose of this work is to fabricate formamidinium-based FA_{0.95}Cs_{0.05}PbI₃ perovskite crystals with added Ge (FA_{0.95}Cs_{0.05}Pb_{1-x}Ge_xI₃) to reduce the amount of Pb and to investigate the microstructures and device performance. Since it was difficult to dissolve germanium iodide (GeI₂) in *N,N*-dimethylformamide and dimethyl sulfoxide solvents, a small amount of CH₃NH₃Cl (MACl) was added to the precursor solutions to improve the



Academic Editor: Chiara Dionigi

Received: 4 October 2024

Revised: 23 December 2024

Accepted: 5 January 2025

Published: 7 January 2025

Citation: Enomoto, A.; Suzuki, A.; Oku, T.; Shimada, H. Promoted Formation of Photoactive α -Formamidinium Cesium Lead Triiodide Perovskite Crystals by Germanium Addition. *Inorganics* **2025**, *13*, 15. <https://doi.org/10.3390/inorganics13010015>

Copyright: © 2025 by the authors. Licensee MDPI, Basel, Switzerland. This article is an open access article distributed under the terms and conditions of the Creative Commons Attribution (CC BY) license (<https://creativecommons.org/licenses/by/4.0/>).

solubility of Ge [18] in the present work. Although Ge addition has already been reported in the previous work [15], the novelty of this study lies in the following three points: (1) the composition of the FA-Cs is different and the Cs composition was minimized in the present work; (2) the DPPS cap layer was not used in the present work, aiming for a stable structure without the cap layer; and (3) the amount of Ge addition was examined in an expanded scale to 40%.

2. Experimental Procedures

The basic process of fabricating perovskite solar cells is illustrated in Figure 1, as reported in the previous work [19]. F-doped tin oxide (FTO, Nippon Sheet Glass Company, Tokyo, Japan, $\sim 10 \Omega/\square$) substrates were cleaned with methanol and acetone in an ultrasonic bath and an ultraviolet ozone cleaner. Precursor solutions of 0.15 and 0.30 M for compact TiO_2 layers were prepared from 1-butanol (Fujifilm Wako Pure Chemical Corporation, Osaka, Japan) and titanium diisopropoxide bis(acetylacetonate) (Sigma-Aldrich, Tokyo, Japan). These precursor solutions of compact TiO_2 were spin-coated on the FTO substrate at 3000 rpm for 30 s and the substrates were heated at 125°C for 5 min. Then, the FTO substrate was annealed at 450°C for 30 min to form a compact TiO_2 layer. To form the mesoporous TiO_2 layer, TiO_2 paste was prepared by mixing TiO_2 powder (Aerosil, Tokyo, Japan, P-25, 200 mg) and poly (ethylene glycol) (Nacalai Tesque, Kyoto, Japan, 20 mg) with ultrapure water (1 mL). To this solution, acetylacetone (Fujifilm Wako Pure Chemical Corporation, 20 μL) and surfactant (Sigma-Aldrich, Triton X-100, 10 μL) were added, mixed for 30 min, and then allowed to stand for 24 h to remove bubbles in the solution. The TiO_2 paste was then spin-coated on the compact TiO_2 layer at 5000 rpm for 30 s. The resulting substrates were heated at 125°C for 5 min and then annealed at 450°C for 30 min to form a mesoporous TiO_2 layer.

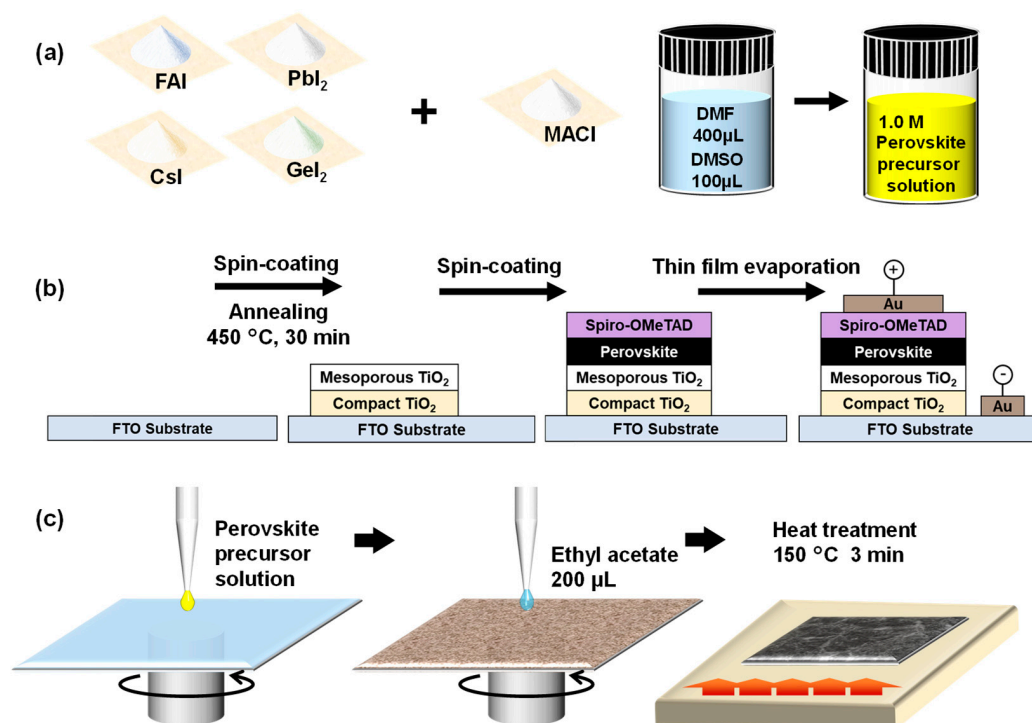


Figure 1. Schematic illustration of the process used to fabricate the perovskite solar cells. (a) Preparation of precursor solutions. (b) Fabrication of solar cell devices. (c) Formation of perovskite films.

To form the perovskite compounds, mixture precursor solutions (1 M) were prepared by dissolving formamidinium iodide (FAI, Sigma-Aldrich), CsI (Daiichi Kigenso Kagaku

Kogyo Co., Tokyo, Japan, Ltd., 6.5 mg), PbI₂ (Sigma-Aldrich), GeI₂ (Sigma-Aldrich), and MAcl (Showa Chemicals, Tokyo, Japan, 13.5 mg) with the desired molar ratio in N,N-dimethylformamide (DMF, Nacalai Tesque, 0.4 mL):dimethyl sulfoxide (DMSO, Tokyo Chemical Industry Co., Ltd., Tokyo, Japan, 0.1 mL), and heated and stirred at 60 °C for 12 h, as illustrated in Figure 1a and Table 1. MAcl was also added to facilitate the dissolution of Ge [18]. Since an ionic radius of Ge²⁺ is smaller than Pb²⁺, MA⁺ and Cl[−] with smaller ionic radii compared with FA⁺ and I[−], respectively, would be more suitable to facilitate the dissolution of Ge to satisfy the suitable tolerance factors. All procedures such as powder preparations and spin-coatings of perovskite solutions were performed in air at a temperature of 22 °C and humidity of ~30%.

Table 1. Compositions of reagents for perovskite precursor solutions.

Ge (%)	Solution Composition	FAI (mg)	PbI ₂ (mg)	GeI ₂ (mg)	MAcl (mg)
0	FA _{0.95} Cs _{0.05} PbI ₃	81.7	230.5	0.0	13.5
8	FA _{0.95} Cs _{0.05} Pb _{0.92} Ge _{0.08} I ₃	81.7	212.1	13.1	13.5
12.5	FA _{0.95} Cs _{0.05} Pb _{0.875} Ge _{0.125} I ₃	81.7	201.7	20.4	13.5
20	FA _{0.95} Cs _{0.05} Pb _{0.80} Ge _{0.20} I ₃	81.7	184.4	32.6	13.5
30	FA _{0.95} Cs _{0.05} Pb _{0.7} Ge _{0.30} I ₃	81.7	161.4	49.0	13.5
40	FA _{0.95} Cs _{0.05} Pb _{0.60} Ge _{0.40} I ₃	81.7	138.3	65.3	13.5

The perovskite solution was dropped onto the TiO₂ film and the film was formed at a rotation speed of 4000 rpm for 30 s. Then, the perovskite solution was dropped and spin-coated again. A solution of ethyl acetate (200 µL) was dropped onto the perovskite layer 10 s before the end of the spinning [20]. The deposited films were then heated at 150 °C for 3 min. Spiro-OMeTAD (Sigma-Aldrich) solution was then spin-coated on the perovskite layer at 4000 rpm for 30 s. Finally, a gold (Au) electrode was deposited to serve as the top electrode. The prepared perovskite solar cells were also stored in air at a temperature of 22 °C and humidity below 30% in a dark room.

The current density–voltage (*J*–*V*) curves of the photovoltaic cells were obtained under illumination of 100 mW cm^{−2} using an AM1.5 solar simulator (San-ei Electric, Osaka, Japan, XES-301S). The solar cells were illuminated through the side of the FTO substrates and the illuminated area was 0.040 cm². The average power conversion efficiency (η_{ave}) values were calculated from the average of six cells. Crystal structures were investigated by X-ray diffraction (XRD) using a diffractometer (Bruker, Billerica, MA, USA, D2 Phaser). Surface structures of the cells were investigated by scanning electron microscopy (SEM, Jeol, Tokyo, Japan, JSM-6010PLUS/LA) equipped with energy-dispersive X-ray spectroscopy (EDX).

3. Results and Discussion

Figure 2 shows photographs of the perovskite films during annealing at 150 °C for 3 min. The color of the devices with added Ge higher than 8% became black. At the initial stage of the annealing, the color of the film turned black, which would indicate precipitation of perovskite crystals. For the perovskite film with added 12.5% Ge, the color of the surface was semitransparent red brown. The red brown color would be due to a mixture of yellow δ -phase and black α -phase. Although surfaces of the perovskite films with added 8~20% Ge were smooth, the perovskite film with added 30% Ge provided inhomogeneous change of the color between the center and outside of the film, which might be due to insufficient annealing conditions or a delicate process of anti-solvent dripping. The yellow region at the center of the perovskite film with added 40% Ge would be the δ -phase, which will be

described in detail for XRD analysis. These photographs indicate that the addition of a suitable amount of Ge promoted the formation of the black α -FAPbI₃.

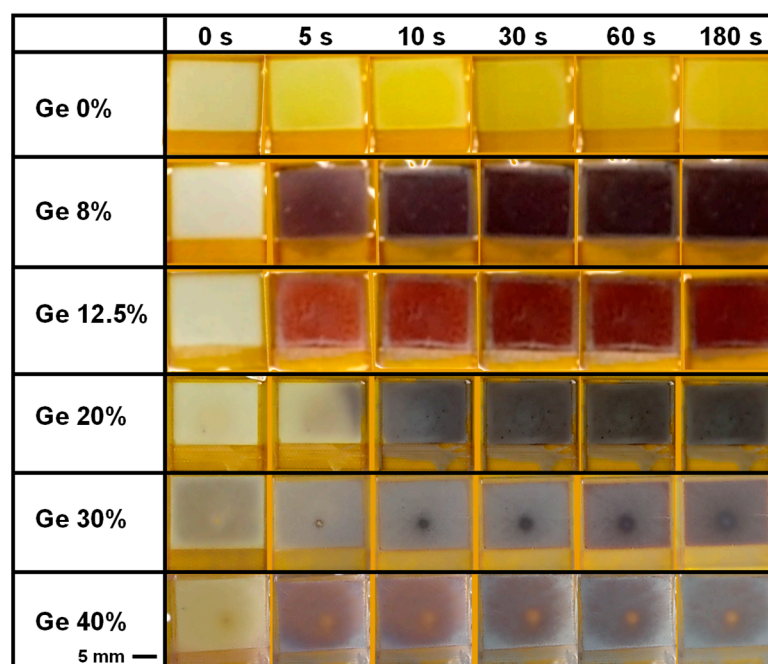


Figure 2. Photographs of Ge-added perovskite films during annealing at 150 °C for 3 min.

Figure 3 shows SEM and elemental mapping images of the present devices. Although there are several particles at the surface in Figure 3a–c, the devices with added 8% and 12.5% Ge exhibited relatively smooth surfaces, and Ge is homogeneously distributed in the matrix of the sample from the elemental mapping images. On the other hand, many particles are distributed over the surface of the device, as observed in Figure 3d,e. The rough surface was observed for the devices with added 30~40% Ge, which might be related with instability of Ge-rich perovskite compounds. The poor performance of these cells would be due to the rough surface of the devices and the performance could be better if the film might be smoother. Magnified SEM and elemental mapping images of FA_{0.95}CS_{0.05}Pb_{0.875}Ge_{0.125}I₃ and FA_{0.95}CS_{0.05}Pb_{0.6}Ge_{0.4}I₃ are shown in Figures 3f and 3g, respectively. EDS analysis of these regions showed the compositions of Ge relative to Pb for FA_{0.95}CS_{0.05}Pb_{0.875}Ge_{0.125}I₃ and FA_{0.95}CS_{0.05}Pb_{0.6}Ge_{0.4}I₃ were 8.0 and 29.7%, respectively. These values are little smaller than those of the preparation compositions, which might be due to the segregation of Ge in the perovskite grains. The elemental mapping images of Figure 3 show that Ge atoms are present in the regions where Pb and I are present, suggesting that Ge is incorporated into the perovskite crystals.

Figure 4 shows XRD patterns of the present devices. The full devices were used for XRD measurements to refine the lattice constants of perovskites using XRD peaks of Au electrodes. For the FA_{0.95}CS_{0.05}PbI₃ without Ge, a strong peak of δ -phase is observed and α -phase is not observed. With increasing the Ge amount, peak intensities of the α -phase gradually increased, as indicated by the yellow highlight.

The XRD results show that the yellow phase observed for the Ge 0% device in Figure 2 corresponds to the δ -phase and the black phase observed for Ge 8% device in Figure 2 corresponds to the α -phase. When the addition of Ge is over 20%, XRD peaks of the δ -phase and PbI₂ disappeared and clear XRD peaks of α -phase were obtained. A peak of δ -phase appeared again when the amount of Ge addition reached 40%, which corresponds to the yellow δ -phase observed at the center of the substrate in Figure 2. Since the XRD data were obtained from a 10 mm size region, an area that contained the yellow spot is included in the

XRD data and the yellow spot would be from the δ -phase. Results of optical microscopy in Figure 2 show that a black α -phase is obtained for the device with 8% Ge but not for that with 12.5% Ge, and a black α -phase appeared again for the device with 20% Ge. The XRD shows similar results, and the formation of the black α -phase and disappearance of the δ -phase for the Ge 20% might be related to the formation of the PbI₂ phase observed in the XRD. Since the Gibbs free energy of the δ -FAPbI₃ is lower than that of α -FAPbI₃ [21], ordinary annealing of the devices in air provided formation of the δ -FAPbI₃.

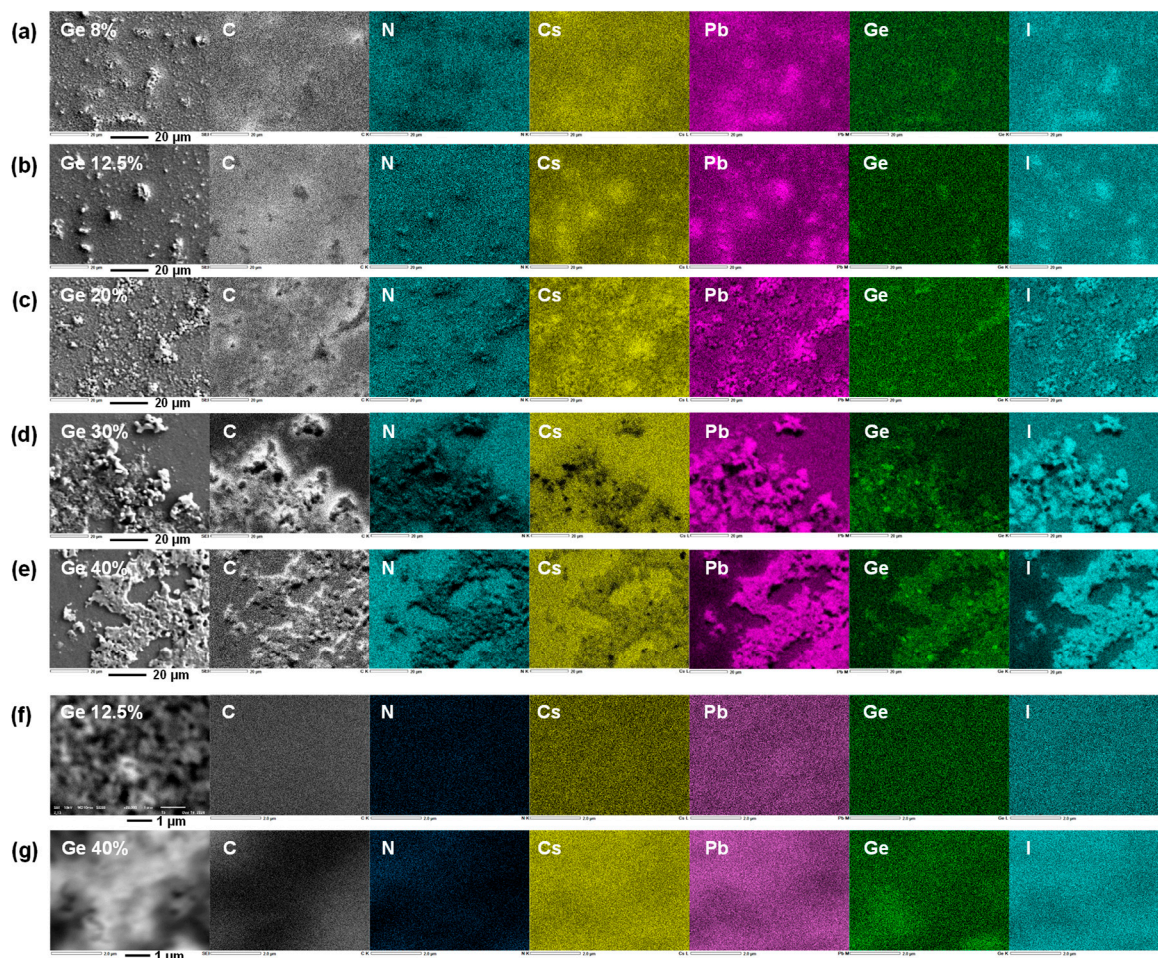


Figure 3. SEM and elemental mapping images of (a) $\text{FA}_{0.95}\text{Cs}_{0.05}\text{Pb}_{0.92}\text{Ge}_{0.08}\text{I}_3$, (b) $\text{FA}_{0.95}\text{Cs}_{0.05}\text{Pb}_{0.875}\text{Ge}_{0.125}\text{I}_3$, (c) $\text{FA}_{0.95}\text{Cs}_{0.05}\text{Pb}_{0.8}\text{Ge}_{0.2}\text{I}_3$, (d) $\text{FA}_{0.95}\text{Cs}_{0.05}\text{Pb}_{0.7}\text{Ge}_{0.3}\text{I}_3$, and (e) $\text{FA}_{0.95}\text{Cs}_{0.05}\text{Pb}_{0.6}\text{Ge}_{0.4}\text{I}_3$. Magnified images of (f) $\text{FA}_{0.95}\text{Cs}_{0.05}\text{Pb}_{0.875}\text{Ge}_{0.125}\text{I}_3$ and (g) $\text{FA}_{0.95}\text{Cs}_{0.05}\text{Pb}_{0.6}\text{Ge}_{0.4}\text{I}_3$.

The best J - V characteristics of the present devices are shown in Figure 5a and the photovoltaic parameters are listed in Table 2. Photovoltaic parameters are indicated as follows: V_{OC} : open-circuit voltage, J_{SC} : short-circuit current density, FF: fill factor, η : conversion efficiency, η_{ave} : average efficiency of six cells. The highest conversion efficiency of 5.74% was obtained for the device with added 12.5% Ge. When the amount of Ge addition was over 20%, the conversion efficiency rapidly decreased to 0.2%, which would be due to decrease of J_{SC} values caused by the leakage currents from the reduced surface flatness of the thin films. Although higher conversion efficiencies were obtained for the device with added Ge 8% compared with the device with Ge-rich phase. XRD intensity of (100) reflection for the Ge 8% device was not higher than those of Ge-rich phase. This would be due to the smoother surface structure of the Ge 8% device compared to the Ge-rich device, which lead to an increase in the J_{SC} values.

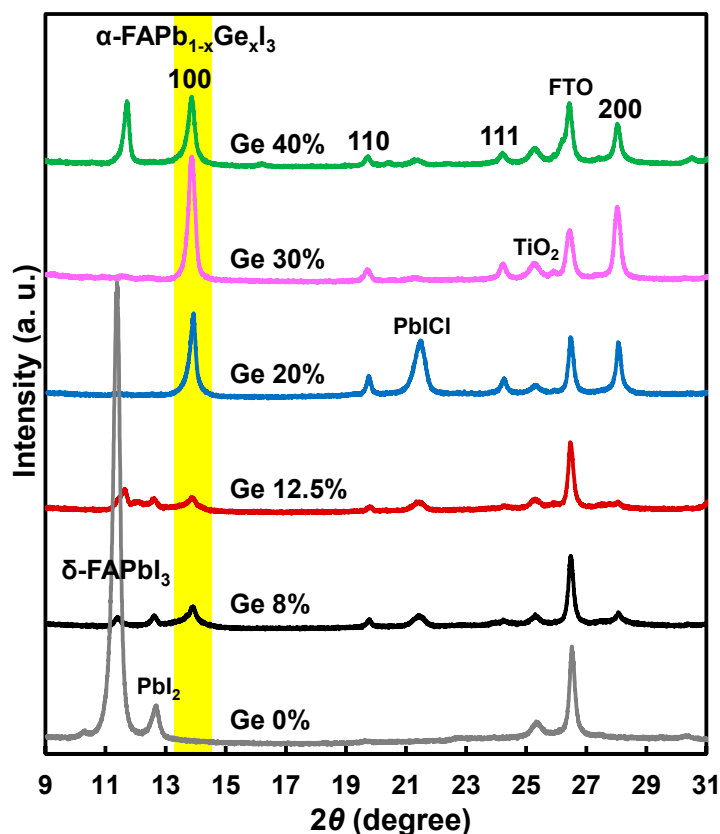


Figure 4. XRD patterns of the present perovskite solar cells.

Table 2. Measured photovoltaic parameters and lattice constants (a) of the as-prepared perovskite photovoltaic devices.

Devices Ge (%)	J_{sc} (mA cm^{-2})	V_{OC} (V)	FF	η (%)	η_{ave} (%)	a (Å)
8	15.5	0.641	0.581	5.74	4.26	6.354(1)
12.5	12.4	0.705	0.659	5.74	5.56	6.355(1)
20	5.61	0.323	0.247	0.448	0.250	6.354(0)
30	1.28	0.415	0.292	0.155	0.0923	6.362(8)
40	1.78	0.451	0.258	0.207	0.0989	6.361(1)
After 2 days						
8	16.5	0.615	0.557	5.66	4.24	-
12.5	12.8	0.716	0.657	6.05	5.87	-
20	8.62	0.491	0.274	1.76	0.957	-
After 7 days						
8	16.0	0.566	0.527	4.78	3.91	-
12.5	12.5	0.704	0.643	5.66	5.48	-
20	9.39	0.540	0.421	2.14	1.45	-
After 21 days						
8	15.9	0.532	0.509	4.31	3.76	-
12.5	12.6	0.694	0.627	5.48	4.93	-
20	9.70	0.472	0.380	1.74	1.38	-
After 34 days						
30	2.83	0.545	0.311	0.479	0.303	-
40	3.93	0.460	0.232	0.420	0.166	-
After 61 days						
8	15.4	0.573	0.535	4.72	4.23	-
12.5	11.6	0.684	0.616	4.87	4.49	-
20	10.2	0.516	0.418	2.20	1.62	-

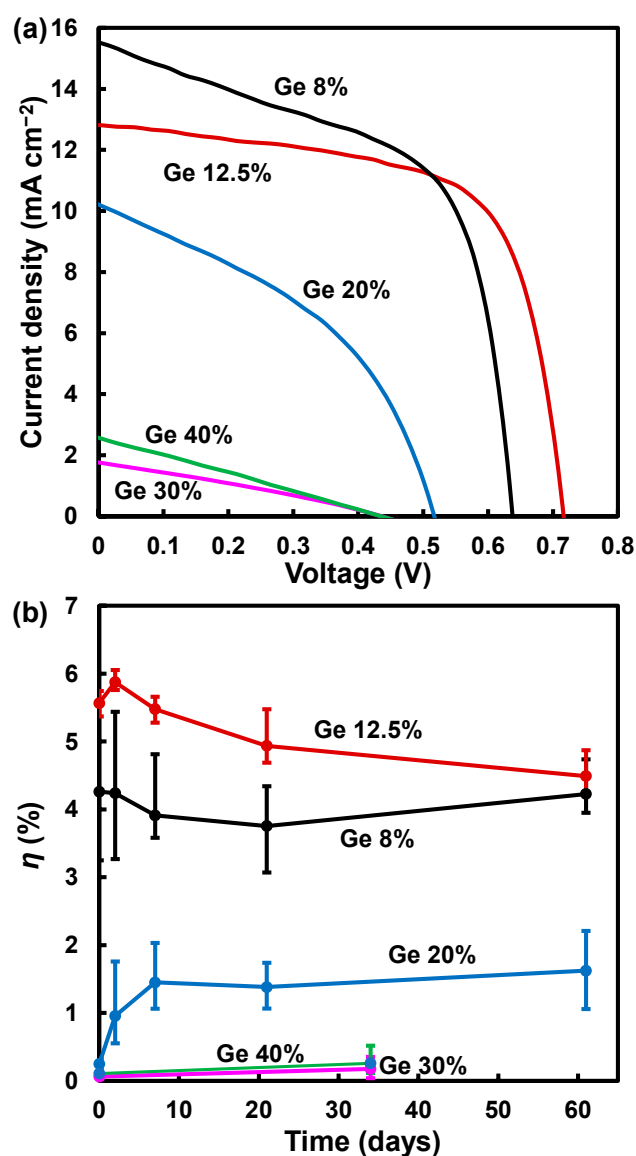


Figure 5. (a) The best J - V characteristics collected in light condition for the fabricated solar cells. (b) Changes of conversion efficiencies as a function of time.

Changes of conversion efficiencies are shown in Figure 5b. Although the conversion efficiencies of the devices with added 8% Ge decreased after 21 days, they increased after 61 days. On the other hand, the efficiency of the device with added 12.5% Ge increased to 6.05% after 2 days in the air atmosphere. This type of efficiency increase has been sometimes observed [22,23] and the lattice defects due to FA or I might be filled by the atomic diffusion during the room temperature aging.

A structure model and electron density distributions of $\text{FA}_{0.875}\text{Cs}_{0.125}\text{Pb}_{0.875}\text{Ge}_{0.125}\text{I}_3$ are shown in Figures 6a and 6b, respectively. The electronic structures of the perovskite crystal were calculated using the density functional theory based on Vanderbilt ultrasoft pseudopotentials and scalar relativistic generalized gradient approximations (Quantum Espresso, v.5.2.1) [24,25]. The electron densities around the Ge-I are lower than those of Pb-I and the electron densities around the Cs are also different from those of FA, which could contribute to the electronic properties of the perovskites. Charge transfer from 5p orbital of the I to 4p orbital of the Ge would contribute carrier transfer and improvement of the J_{SC} . Differences of total energies between α - and δ -phases are calculated to be -1.4 eV and -1.2 eV for $\text{FA}_{0.875}\text{Cs}_{0.125}\text{PbI}_3$ and Ge-added $\text{FA}_{0.875}\text{Cs}_{0.125}\text{Pb}_{0.875}\text{Ge}_{0.125}\text{I}_3$, respectively. This

indicates the Ge-doping could reduce the energy difference between α - and δ -phases, which would lead to the stability of the Ge-added perovskites. Calculated band structures and partial density of states (pDOS) of $\text{FA}_{0.875}\text{Cs}_{0.125}\text{Pb}_{0.875}\text{Ge}_{0.125}\text{I}_3$ are shown in Figure 6c and Figure 6d, respectively. Energy gaps of $\text{FA}_{0.875}\text{Cs}_{0.125}\text{PbI}_3$ and $\text{FA}_{0.875}\text{Cs}_{0.125}\text{Pb}_{0.875}\text{Ge}_{0.125}\text{I}_3$ are calculated to be 0.994 and 0.920 eV, respectively. The 6p orbital of the Pb atom and 4p orbital of the Ge atom are overlapping and dominate in the conduction band, which would contribute to the improvement of carrier transfer in the Ge-doped FACsPbI₃.

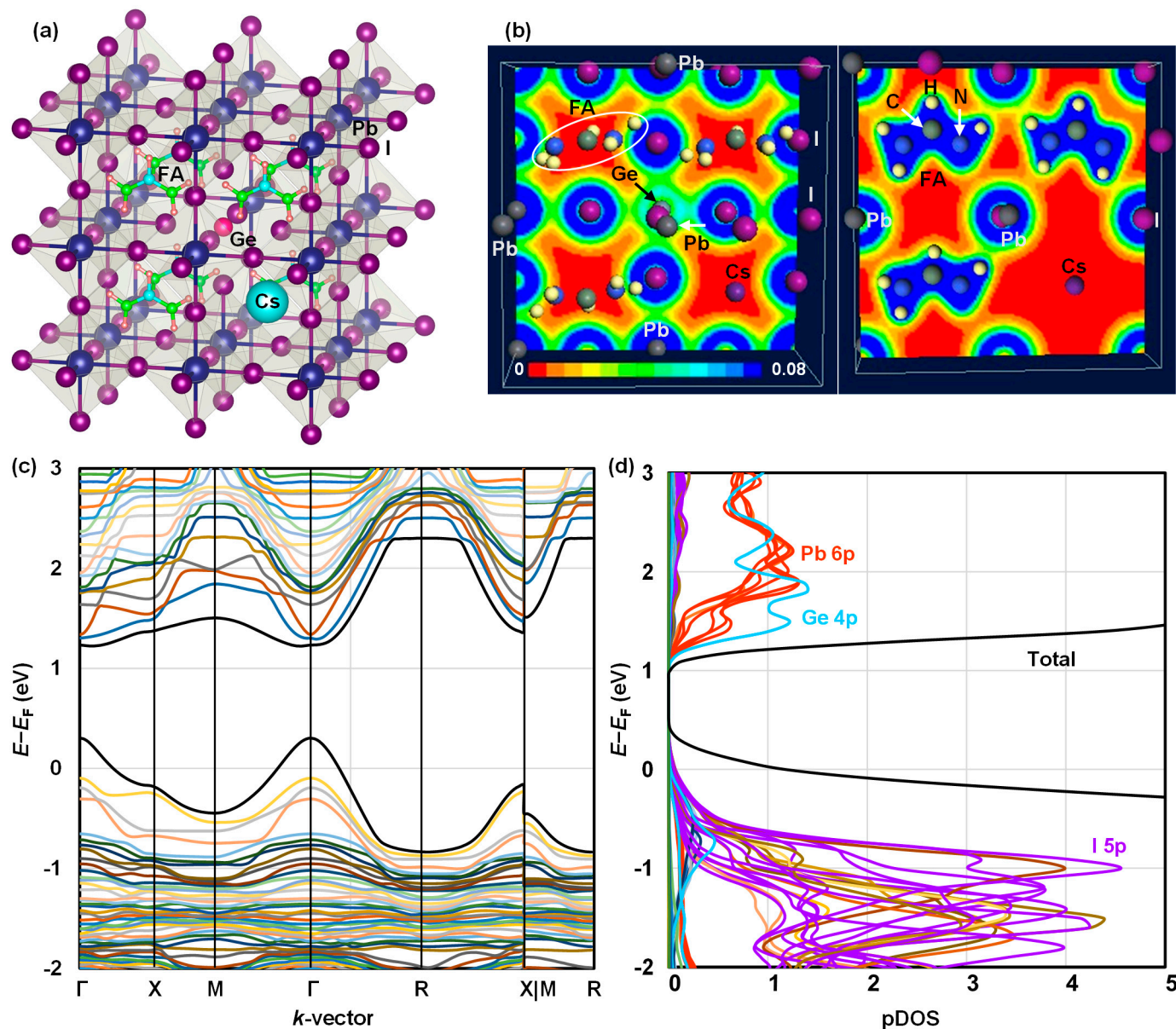


Figure 6. (a) Structure model, (b) electron density distributions (different slices), (c) band structures, and (d) partial density of states of $\text{FA}_{0.875}\text{Cs}_{0.125}\text{Pb}_{0.875}\text{Ge}_{0.125}\text{I}_3$.

In the previously reported work [18], the η values drastically decreased from 22% to 5% by adding 7% Ge to $\text{FA}_{0.83}\text{MA}_{0.17}\text{Pb}(\text{I}_{0.9}\text{Br}_{0.1})_3$. On the other hand, in the present work, devices consisting of $\text{FA}_{0.95}\text{Cs}_{0.05}\text{PbI}_3$ with added 8~40% Ge were fabricated in air and characterized, and the highest efficiency of 6.05% was obtained for the device with 12.5% Ge. In addition, α -phase of $\text{FA}_{0.95}\text{Cs}_{0.05}\text{PbI}_3$ crystals were stabilized by adding 20~40% Ge, which indicated the possibility of Ge as an alternative element of Pb. Further characterizations by transmission electron microscopy, space-charge-limited current measurements,

and time-resolved photoluminescence are needed to understand the microstructures and defect states of the Ge-added perovskite crystals. Although it was reported that additions of monovalent copper could also promote formation of the α -FAPbI₃ [25], the monovalent copper would occupy at the FA site, which is different from the present results on the Ge at the Pb site. For the future work, combination of monovalent and divalent metal cations might be effective to stabilize the α -FAPbI₃. Conversion efficiencies of solar cells fabricated based on pure CsPbI₃ also reached 23% [26]. Recently, pure CsPbI₃ with an efficiency of 21.8% retains 97% of the initial conversion efficiency after operation under continuous illumination for 440 h [27]. Further studies are expected on the CsPbI₃.

4. Conclusions

Perovskite solar cells with the compositions of FA_{0.95}Cs_{0.05}Pb_{1-x}Ge_xI₃ ($x = 0\text{--}0.4$) were fabricated and their microstructures and photovoltaic properties were characterized. With increasing the amounts of Ge, XRD intensities of (100) reflection of the α -phase increased, which indicates the effectiveness of the Ge addition to form the α -phase. The highest conversion efficiency of 6.05% was obtained for the device with added 12.5% Ge after 2 days. Conversion efficiencies of the device with added 20% Ge increased from 0.2 to 2.0% after 7 days and were almost stable for 61 days. The elemental mapping images showed that Ge atoms are present in the regions where Pb and I are present, suggesting that Ge is incorporated into the perovskite crystals.

Author Contributions: Conceptualization, A.E., A.S. and T.O.; methodology, A.E., A.S. and T.O.; formal analysis, A.E., A.S. and T.O.; investigation, A.E., A.S., T.O. and H.S.; writing—original draft preparation, A.E. and T.O.; writing—review and editing, A.E., A.S., T.O. and H.S.; project administration, A.S. and T.O.; funding acquisition, A.S. and T.O. All authors have read and agreed to the published version of the manuscript.

Funding: This work was partly funded by Japan Society for the Promotion of Science as a Grant-in-Aid for Scientific Research KAKENHI (C) 21K04809 and KAKENHI (C) 21K05261.

Institutional Review Board Statement: Not applicable.

Informed Consent Statement: Not applicable.

Data Availability Statement: Data are contained within the article.

Acknowledgments: The authors would like to acknowledge Takahiro Kamo, Daiichi Kigenso Kagaku Kogyo Co., Ltd., for providing CsI.

Conflicts of Interest: The authors declare no conflicts of interest.

References

1. Zhang, H.; Ji, X.; Yao, H.; Fan, Q.; Yu, B.; Li, J. Review on efficiency improvement effort of perovskite solar cell. *Sol. Energy* **2022**, *233*, 421–434. [[CrossRef](#)]
2. Sharma, R.; Sharma, A.; Agarwal, S.; Dhaka, M.S. Stability and efficiency issues, solutions and advancements in perovskite solar cells: A review. *Sol. Energy* **2022**, *244*, 516–535. [[CrossRef](#)]
3. Park, J.; Kim, J.; Yun, H.-S.; Paik, M.J.; Noh, E.; Mun, H.J.; Kim, M.G.; Shin, T.J.; Seok, S.I. Controlled growth of perovskite layers with volatile alkylammonium chlorides. *Nature* **2023**, *616*, 724–730. [[CrossRef](#)] [[PubMed](#)]
4. Najarian, M.; Dinic, F.; Chen, H.; Sabatini, R.; Zheng, C.; Lough, A.; Maris, T.; Saidaminov, M.I.; García de Arquer, F.P.; Voznyy, O.; et al. Homomeric chains of intermolecular bonds scaffold octahedral germanium perovskites. *Nature* **2023**, *620*, 328–335. [[CrossRef](#)]
5. Rao, M.K.; Sangeetha, D.N.; Selvakumar, M.; Sudhakar, Y.N.; Mahesha, M.G. Review on persistent challenges of perovskite solar cells' stability. *Sol. Energy* **2021**, *218*, 469–491. [[CrossRef](#)]
6. Magdalin, A.E.; Nixon, P.D.; Jayaseelan, E.; Sivakumar, M.; Devi, S.K.N.; Subathra, M.S.P.; Kumar, N.M.; Ananthi, N. Development of lead-free perovskite solar cells: Opportunities, challenges, and future technologies. *Results Eng.* **2023**, *20*, 101438. [[CrossRef](#)]
7. Oku, T. Crystal structures of perovskite halide compounds used for solar cells. *Rev. Adv. Mater. Sci.* **2020**, *59*, 264–305. [[CrossRef](#)]

8. Bu, T.; Li, J.; Li, H.; Tian, C.; Su, J.; Tong, G.; Ono, L.K.; Wang, C.; Lin, Z.; Chai, N.; et al. Lead halide-templated crystallization of methylamine-free perovskite for efficient photovoltaic modules. *Science* **2021**, *372*, 1327–1332. [[CrossRef](#)] [[PubMed](#)]
9. Chen, S.; Pan, L.; Ye, T.; Lei, N.; Yang, Y.; Wang, X. The lattice reconstruction of Cs-introduced FAPb_{1.80}Br_{1.20} enables improved stability for perovskite solar cells. *RSC Adv.* **2021**, *11*, 3997–4005. [[CrossRef](#)] [[PubMed](#)]
10. Khadka, D.B.; Shirai, Y.; Yanagida, M.; Tadano, T.; Miyano, K. Interfacial embedding for high-efficiency and stable methylammonium-free perovskite solar cells with fluoroarene hydrazine. *Adv. Energy Mater.* **2022**, *12*, 2202029. [[CrossRef](#)]
11. Jeong, J.; Kim, M.; Seo, J.; Lu, H.; Ahlawat, P.; Mishra, A.; Yang, Y.; Hope, M.A.; Eickemeyer, F.T.; Kim, M.; et al. Pseudo-halide anion engineering for α -FAPbI₃ perovskite solar cells. *Nature* **2021**, *592*, 381–385. [[CrossRef](#)] [[PubMed](#)]
12. Chen, H.; Chen, Y.; Zhang, T.; Liu, X.; Wang, X.; Zhao, Y. Advances to high-performance black-phase FAPbI₃ perovskite for efficient and stable photovoltaics. *Small Struct.* **2021**, *2*, 2000130. [[CrossRef](#)]
13. Masi, S.; Gualdrón-Reyes, A.F.; Mora-Seró, I. Stabilization of Black Perovskite Phase in FAPbI₃ and CsPbI₃. *ACS Energy Lett.* **2020**, *5*, 1974–1985. [[CrossRef](#)]
14. Li, R.; Song, J.; Peng, J.; Tian, X.; Xu, Y.; Huang, H.; Bai, S.; Li, Y.; Yao, F.; Lin, Q. Temperature-dependent performance metrics of tin-doped perovskite photodetectors. *J. Mater. Chem. C* **2022**, *10*, 1625–1631. [[CrossRef](#)]
15. Enomoto, A.; Suzuki, A.; Oku, T.; Fukunishi, S.; Tachikawa, T.; Hasegawa, T. First-principles calculations and device characterizations of formamidiniumcesium lead triiodide perovskite crystals stabilized by germanium or copper. *Jpn. J. Appl. Phys.* **2023**, *62*, SK1015. [[CrossRef](#)]
16. Kogo, A.; Yamamoto, K.; Murakami, T.N. Germanium ion doping of CsPbI₃ to obtain inorganic perovskite solar cells with low temperature processing. *Jpn. J. Appl. Phys.* **2022**, *61*, 020904. [[CrossRef](#)]
17. Yang, F.; Hirotsu, D.; Kapil, G.; Kamarudin, M.A.; Ng, C.H.; Zhang, Y.; Shen, Q.; Hayase, S. All-inorganic CsPb_{1-x}Ge_xI₂Br perovskite with enhanced phase stability and photovoltaic performance. *Angew. Chem. Int. Ed.* **2018**, *57*, 12745–12749. [[CrossRef](#)] [[PubMed](#)]
18. Kim, G.M.; Ishii, A.; Öz, S.; Miyasaka, T. MAI-assisted Ge doping of Pb-hybrid perovskite: A universal route to stabilize high performance perovskite solar cells. *Adv. Energy Mater.* **2020**, *10*, 1903299. [[CrossRef](#)]
19. Oku, T.; Ohishi, Y.; Ueoka, N. Highly (100)-oriented CH₃NH₃PbI₃(Cl) perovskite solar cells prepared with NH₄Cl using an air blow method. *RSC Adv.* **2018**, *8*, 10389–10395. [[CrossRef](#)]
20. Zhang, W.; Li, Y.; Liu, X.; Tang, D.; Li, X.; Yuan, X. Ethyl acetate green antisolvent process for high-performance planar low-temperature SnO₂-based perovskite solar cells made in ambient air. *Chem. Eng. J.* **2020**, *379*, 122298. [[CrossRef](#)]
21. Liu, X.; Luo, D.; Lu, Z.-H.; Yun, J.S.; Saliba, M.; Seok, S.I.; Zhang, W. Stabilization of photoactive phases for perovskite photovoltaics. *Nat. Rev. Chem.* **2023**, *7*, 462–479. [[CrossRef](#)] [[PubMed](#)]
22. Oku, T.; Taguchi, M.; Suzuki, A.; Kitagawa, K.; Asakawa, Y.; Yoshida, S.; Okita, M.; Minami, S.; Fukunishi, S.; Tachikawa, T. Effects of polysilane addition to chlorobenzene and high temperature annealing on CH₃NH₃PbI₃ perovskite photovoltaic devices. *Coatings* **2021**, *11*, 665. [[CrossRef](#)]
23. Ono, I.; Oku, T.; Genko, Y.; Okumura, R.; Nasu, T.; Mizuno, S.; Tachikawa, T.; Hasegawa, T.; Fukunishi, S. Stable decaphenylcyclopentasilane hole transport layers for double-stacked perovskite photovoltaic devices fabricated under ambient atmosphere. *Chem. Inorg. Mater.* **2024**, *4*, 100066. [[CrossRef](#)]
24. Kuo, Y.-C.; Oku, T.; Suzuki, A.; Ono, I.; Okumura, R. Electronic structures of lead-free Sn- or Ge-hybrid perovskite halides studied by first-principles calculation. *Hybrid Adv.* **2024**, *5*, 100174. [[CrossRef](#)]
25. Okumura, R.; Oku, T.; Suzuki, A. Accelerated formation of photoactive formamidinium-based lead triiodide perovskite crystals by the addition of copper iodide. *Chem. Inorg. Mater.* **2024**, *3*, 100052. [[CrossRef](#)]
26. Zhang, T.; Chen, Y.; Kan, M.; Xu, S.; Miao, Y.; Wang, X.; Ren, M.; Chen, H.; Liu, X.; Zhao, Y. MA cation-induced diffusional growth of low-bandgap FA-Cs perovskites driven by natural gradient annealing. *Research* **2021**, *2021*, 9765106. [[CrossRef](#)] [[PubMed](#)]
27. Yang, S.; Wu, M.; Lei, X.; Wang, J.; Han, Y.; He, X.; Liu, S.; Liu, Z. Ultra-high 1.27 V V_{OC} of pure CsPbI₃ perovskite solar cells with an efficiency of 21.8%. *ACS Energy Lett.* **2024**, *9*, 4817–4826. [[CrossRef](#)]

Disclaimer/Publisher's Note: The statements, opinions and data contained in all publications are solely those of the individual author(s) and contributor(s) and not of MDPI and/or the editor(s). MDPI and/or the editor(s) disclaim responsibility for any injury to people or property resulting from any ideas, methods, instructions or products referred to in the content.